IEEE Access
Multidisciplinary ⋮ Rapid Review ⋮ Open Access Journal

Date of publication xxxx 00, 0000, date of current version xxxx 00, 0000.

Digital Object Identifier 10.1109/ACCESS.2022.Doi Number

Modeling of Transcutaneous Recording for Bio-impedance Analysis on the Upper-arm

E. Salkim[1,2], Member, IEEE, Y. Wu[1], Member, IEEE

[1]Department of Electronic and Electrical Engineering, University College London (UCL), Torrington Place, London WC1E 7JE, UK
[2]Department of Electronic and Automation, Mus Alparslan University, Mus, Turkey
Corresponding author: E.Salkim (e.salkim@ ucl.ac.uk, e.salkim@alparslan.edu.tr).
"This work was supported in part by UCL Research Culture Awards 2022."

ABSTRACT Bio-impedance analysis (BIA) is a non-invasive way of assessing body composition. It has been recently adapted for hand motion interpretation with promising results. However, heavily relying on a large number of electrode arrays and learning algorithms, a compact and optimized BIA recording strategy was yet thoroughly investigated. This paper uses computational modeling to facilitate the design of the BIA strategy. An anatomically accurate three dimensional (3D) upper-hand model was developed based on transient finite elements. The model can give helpful insight into the effect of stimulating electrodes at numerous positions on the upper arm, which is otherwise challenging to investigate in practical studies. Different electrode arrangements were designed to obtain the optimal arrangement for the bio-impedance analysis on the upper – arm based on electrical potential and current density distributions over and within the volume conductor. The impedance and phase variation were recorded for different sides of the arm using a systematic procedure based on the optimal electrode arrangement. The results show that the proposed modeling can be used to guided BIA strategy.

INDEX TERMS Bio-impedance analysis, human-machine interface, transient finite element, upper-arm model, volume conductor

I. INTRODUCTION

The most frequently used wearable hand motion interpretation is based on surface electromyography (sEMG), particularly for controlling myoelectric prostheses. Yet sEMG is far from achieving human-like hand motion [1]. This limitation is primarily due to challenges related to sEMG signals. These include limited signal amplitudes of up to tens of mV with frequencies up to about 500 Hz, which are susceptible to noise and low-frequency interference. sEMG also exhibits limited spatial resolution, making the recording of deep muscle activity in the forearm challenging and limiting the number of recognizable degree of freedoms (DOFs) [2]. To address these limitations, alternative non-invasive ways of recording raw bio-signals may provide further advancement in the field.

Bio-impedance analysis (BIA) is a promising approach for assessing body composition that has been recently explored as a human-machine interaction (HMI) method. Similar to sEMG, BIA involves placing electrodes on the skin. However, instead of recording spontaneous neural signals, BIA injects a current and measures resulting voltage potentials. Current-induced voltage signals have a better signal-to-noise ratio (SNR) and are related to the body composition underneath the electrodes. In recent studies, BIA has been shown to be a viable approach for HMI, with the forearm enclosed by a flexible band containing an array of evenly distributed electrodes. The collected BIA dataset is then analyzed using machine learning algorithms to reflect upper limb movement [3], [4].

The placement of electrodes on the skin affects the quality and accuracy of BIA signal acquisition. To optimize the placement of electrodes, several factors need to be considered, including the number of electrodes, the geometry of the electrode array, and the spatial distribution as well as the placement of the electrodes relative to underlying muscle and bone structures [5]– [7].

This paper develops an anatomically accurate human arm model that can be used to investigate the impact of the electrode placement for the BIA strategy. The models are implemented in finite element (FE) models (FEM) involving a volume conductor model representing various anatomical structures and the electrodes by their respective dielectric features and appropriate boundary conditions [8]. It has been shown that the optimal electrode position may be defined

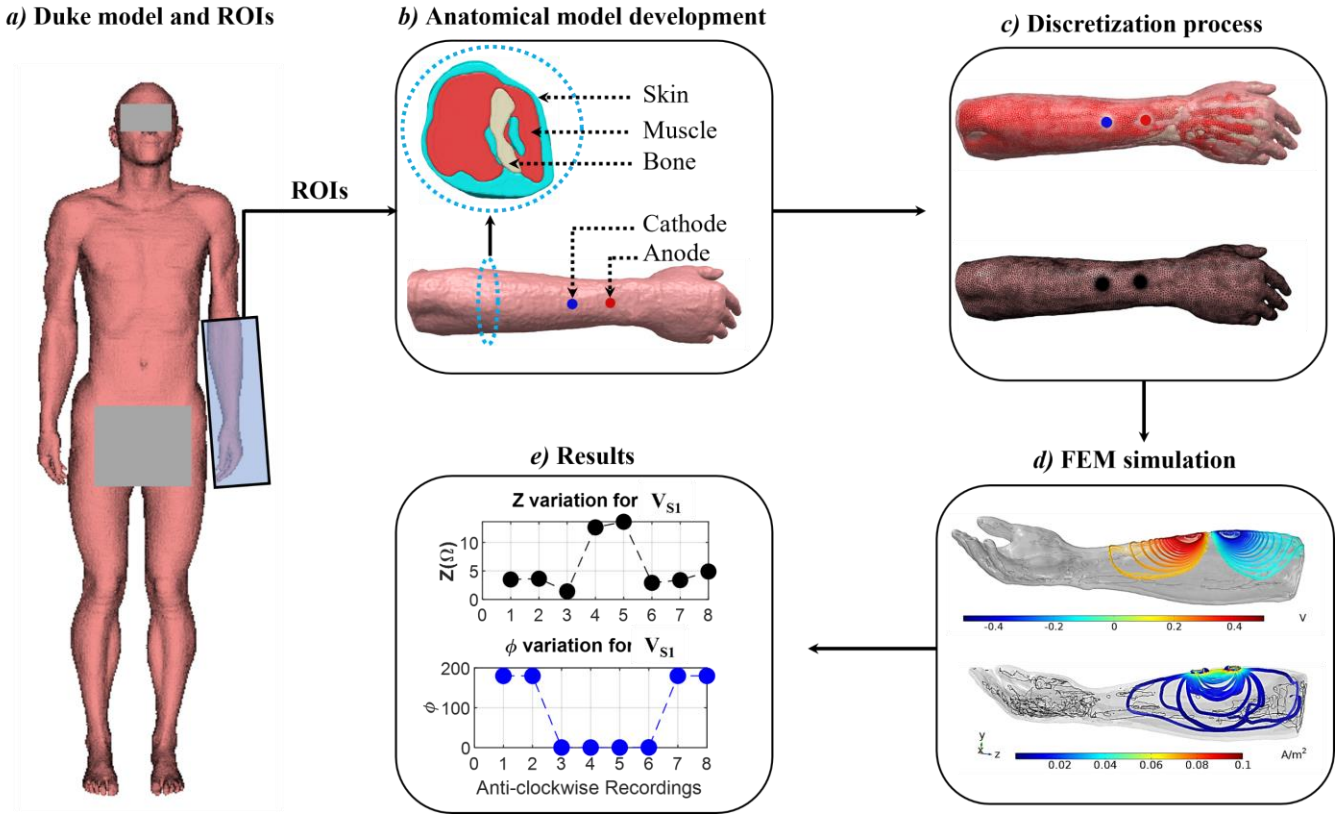

FIGURE 1. **(a) Shows the whole Duke model. (b) Shows region of interest (ROIs) and generation of upper anatomical arm model development. Electrode polarities are highlighted. (c) Shows discretization of the upper arm using appropriate FEM meshing settings. (d) Shows the distribution of the electrical potential within the upper arm based applied current pulse. (e) Shows the impedance (Z) and phase (Φ) variation of different anti-clock recording points over the arm for an electrode arrangement.**

based on electrical potential and current distributions using neuromodulator settings and the electrical properties of the anatomical layers [9], [10]. Thus, in this study, the optimal electrode placement was defined by:

1. Penetrating inner structures with relatively higher and wider magnitudes (e.g., current density).
2. Showing smooth electrical potential and current density variations within and over the model.

The model was generated on the arm of the Duke model, as shown in Fig. 1(a). Two electrodes were placed on the skin layer for current excitation and are denoted as the Cathode and the Anode, as shown in Fig. 1(b). After discretization and simulation, the final bioimpedance can be obtained for analysis.

The paper is organized as follows. Section II presents the method used to develop the model; Section III gives the results of the chosen BIA simulation. The discussion and conclusion are given in Sections IV and V, respectively.

II. METHODS

All models were developed in Simpleware (Synopsys, Mountain View, USA) using the design of the FE tools, and all simulations were carried out using COMSOL Multiphysics (COMSOL, Ltd, Cambridge, UK), which is module-based FE software widely used in physics and engineering design and optimization strategies. The AC/DC and Design modules were used for the electric simulations. The time-based solution method was used to calculate results to analyze the evolution of the impedance variation inside the human upper arm over time. These are detailed as follows.

A. HUMAN ARM ANATOMICAL MODEL DEVELOPMENT

The multi-layered realistic human hand model was generated based on the Duke model of a healthy male subject. Since the model consists of all anatomical layers, the region of interest (ROIs) was separated from the elbow to reduce the computation cost. The whole model was imported to Simpleware, and the region of the interest was separated from the whole body, as shown in Fig. 1(a) and (b). The arm model consists of the fundamental anatomical tissue layers, including skin, muscle, and bone. As each tissue layer was saved as Standard Tessellation Language (STL) surface triangulations, these were converted to the image data to generate accurate and efficient three-dimensional (3D) models using image processing tools. The process of segmentation entails the identification and labeling of the ROIs (e.g., skin, muscles, and bones) and the creation of

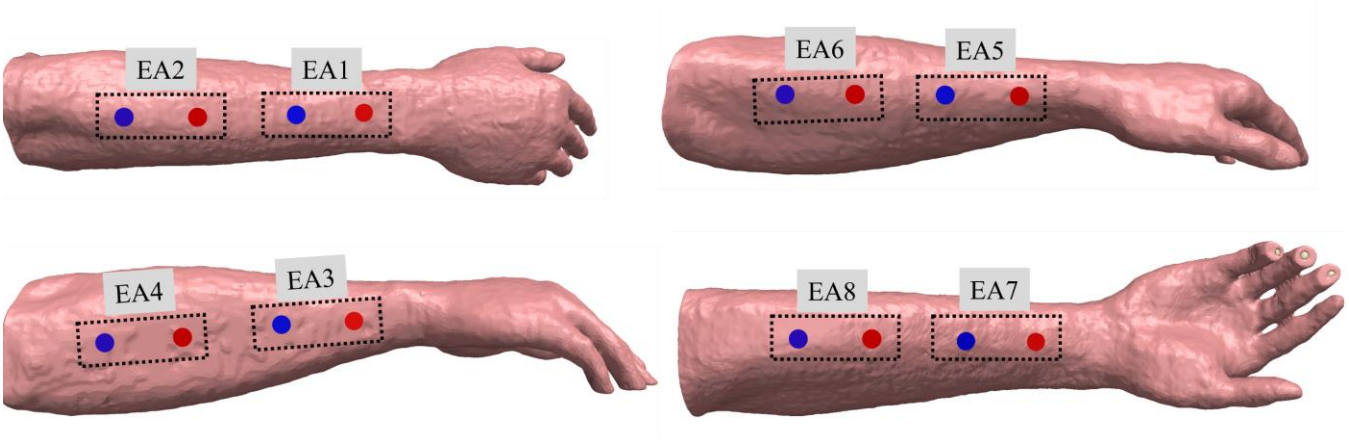

FIGURE 2. **Shows eight different electrode arrangements (EAs) over the arm. Each arrangement is labelled. Two EAs are shown in each arm model. Anode is highlighted in red, and the cathode is highlighted in blue.**

masks [8], [11]. The segmentation process was applied to each mask using automatic image processes, as shown in Fig. 1(b). Manual segmentation was enforced on the anatomical layers and added details where the automation process was insufficient. Then, the morphological image filters (such as *close filter* and *recursive Gaussian* smoothing filters) were applied to the 3D domain of each tissue layer to obtain computationally efficient models. It is noted that the Boolean operations were applied to obtain appropriate boundaries and remove any overlapping sections between the tissue layers. Then, each model was discretized (as shown in Fig. 1(c)), simulated (as shown in Fig. 1(d)) and the results were recorded (as shown in Fig. 1(e)) based on given simulation settings.

B. ELECTRODE DESIGN STRATEGY

After the generation of the upper arm volume conductor, the electrode (the Cathode and the Anode) should be designed to simulate current flows from a stimulating electrode to a return electrode via conductive mediums. It has been shown that the electrode edge effect has a significant impact on patient comfort. High current levels in the sharp edges cause skin damage [12]. Circular geometry is still the gold standard for electrode design and is widely used for neuromodulators. Thus, electrodes were designed using smooth geometrical shapes (e.g., cylinder) and mounted to the human arm model in Simpleware. The radius of each electrode was set to 5 mm. The pitch of electrodes was chosen as 45 mm. Since the muscle layer covers the bony structure from wrist to elbow, electrode configuration was placed in various places on the arm to carry out quantitative comparisons on the effect of stimulating electrodes on the upper arm. Eight different electrode models (as shown in Fig. 2) were designed to investigate the impact of the electrode position placement on the BIA.

It was ensured that each electrode configuration had good contact with the skin to obtain accurate electrical potential distribution within the model. Each electrode model was combined with the anatomical arm model, and the meshing settings were adjusted to generate the FEM model. The most

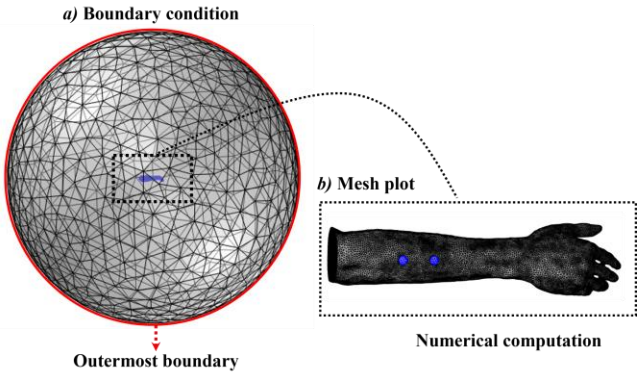

FIGURE 3. **(a) Shows boundary condition. The outermost layer (sphere) is chosen as ground boundary. (b) Represents mesh plot of the arm model using an electrode arrangement.**

detailed geometries were meshed using finer mesh settings to maintain realistic tissue architecture without losing detail through smoothing operations. After adjusting the mesh settings from the model configuration in Simpleware, the model was exported to COMSOL to explore the electrical impedance variation based on given tissue electrical parameters and applied boundary conditions.

C. BOUNDARY CONDITIONS AND DISCRETIZATION

The outermost layer was defined around the models to imitate infinity as shown in Fig. 3(a). The radius of the layer was gradually increased until no significant variation was observed in the electrical potential [8], [11], [13]. Dirichlet boundary condition was applied to the external boundaries of the mentioned sphere using (1). This condition sets potential at the boundaries to zero at infinity [14]. Given the insulation at the boundary of the body, this domain was set to be a non-conductive layer to obtain accurate electrical potential distributions within the volume conductor.

$$V(\delta\Omega) = 0 \tag{1}$$

where $\delta\Omega$ represents the most external boundary and the dielectric parameters of the external layer (sphere) are set according to Table I, and V shows electrical potential.

After defining boundary conditions, it is vital to choose the appropriate discretization settings to obtain accurate simulation results. The tetrahedral meshing setting (as shown in Fig. 3(b)) was used to discretize the models to solve partial differential equations. Since the medium has different geometry, the region of interest (e.g., electrode and upper arm layers) was relatively finer meshed compared to the outermost layer to reduce computation cost. Thus, electrode, skin, muscle, and bone domains were meshed using a minimum element size of 1 µm and a relatively lower growth rate (1.1) to obtain results in a reasonable time. Since the outermost layer (sphere) was far from the region of interest, the tetrahedral element size was selected to be larger by using the *Normal* tetrahedral setting. This resulted in about one million finite elements for each model.

D. TRANSIENT FINITE ELEMENT SIMULATION

Traditionally, tissue impedances have been implemented as pure resistances based on the previous study [15]. It has been shown that the capacitive effect has an impact on the electrical potential distribution within the volume conductor [13], [16]. Thus, the study was designed based on the transient approximation of Maxwell equation (2) shown below:

$$\nabla \cdot \left(\sigma \nabla V - \varepsilon_0 \varepsilon_r \nabla \frac{\partial V}{\partial t}\right) \tag{2}$$

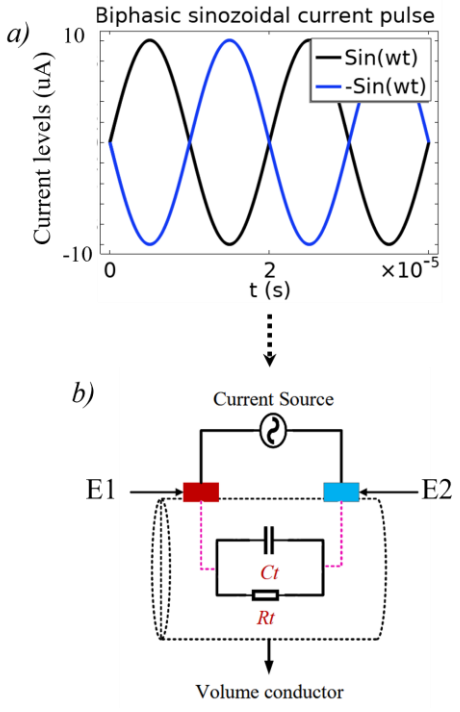

FIGURE 4. (a) Shows the waveform of the differential source current. The anode (E1) current is highlighted in black, and the cathode (E2) is highlighted in blue. (b) Represents the volume conductor of the upper arm and applied the current source using electrode arrangements. Using transient simulation allows for considering the capacitive (Ct) and resistance (Rt) impact of the tissue on the results. Sin(ωt) shows a sinusoidal current pulse.

TABLE I
TISSUE CONDUCTIVITIES

Tissue layer	Conductivity (S/m)	Relative Permittivity (F/m)
Skin	$2.73e^{-4}$	$1.13e^{3}$
Muscle (long.)	0.35	$1.01e^{4}$
Muscle (trans.)	0.105	$4e^{4}$
Bone	0.02	$2.64e^{3}$
Outermost sphere	$10e^{-12}$	1

where σ is the tissue conductivity, V is the electrical potential in the representative geometry, $\varepsilon_0 \varepsilon_r$ is the tissue permittivity, and the values are set according to Table I. ∇ is the Hamiltonian operator. After defining the solution method, an isotropic and homogeneous electrical conductivity value (in S/m) and tissue permittivity was assigned to each sub-domain of each upper arm model based on 50 kHz, as shown in Table I [17]. The wave propagation and inductive effects were assumed to be negligible.

Since it was also aimed to calculate the current density variations within and over the model, the current density was calculated using (3).

$$J = \sigma \cdot E + \frac{\Delta D}{\Delta t} \tag{3}$$

where J represents calculated current density, E indicates eveninduced electrical field and D shows displacement.

The simulation source was designed based on a fully differential sinusoidal waveform based on 50 kHz in COMSOL as shown in Fig. 4(a). After choosing the sinusoidal waveform, the *Analytic* function was applied to the generated waveform to construct a periodic sinusoidal waveform based on the defined frequency magnitude. The periodic sinusoidal current pulse was constructed by choosing the *Sine* parameter and adding angular frequency. Then, the plot parameters were defined using defined frequency, *lower limit*, and *upper limit*. In all the simulated cases, the stimulation current was set up to 10 µA injected from the Anode (red) electrodes and received from the Cathode (blue) electrodes as shown in Fig 4(b). Then, a biphasic wave current pulse with a 10 µA amplitude and a pulse duration of 10 µs was applied to the electrodes for each model. This was implemented in COMSOL by the *terminal current* of negative value for the cathodes and positive value for the anodes. The electrode-tissue interface contact impedance was assumed to be zero for simplicity reasons.

Also, it has been shown that the significant differences in electrical parameters for muscles in a different direction (the axial direction compared to the radial direction) may have a notable influence on the simulation results [16], [18]. Thus, it is essential to include anisotropy of the electrical properties of the associated materials to get a qualitative understanding of the processes involved and accurately interpret the outcome of the simulations accordingly.

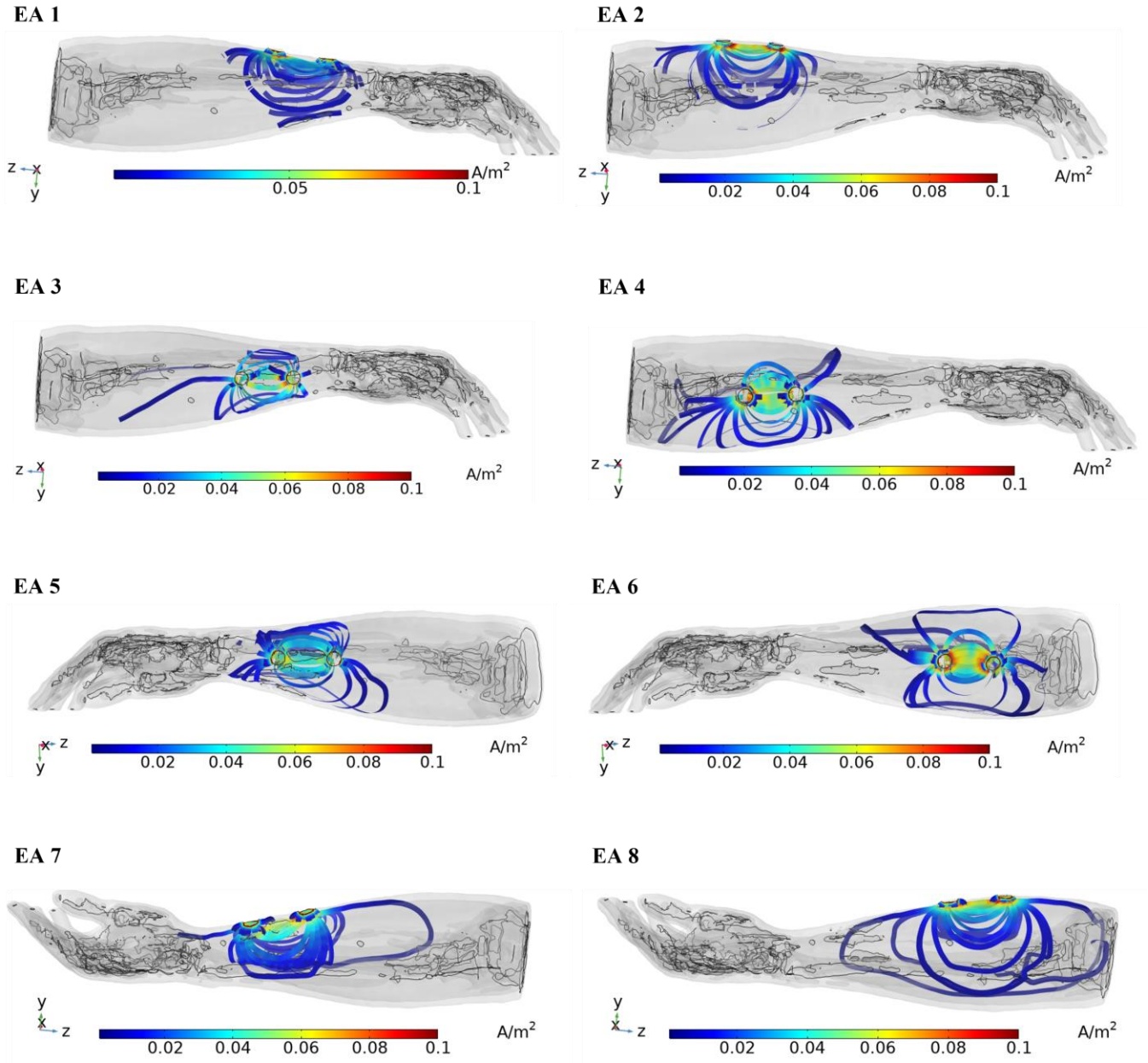

FIGURE 5. **Shows the distributions of the electrical current density variation within the arm model using different electrode arrangements (EAs). The electrical current density distribution streamlines are highlighted for each EA.**

It is noted that the same current pulse with associated level and frequency magnitude was designed and applied to all electrode models for a fair comparison.

III. RESULTS

The first step of this study was to define the optimal electrode arrangements (EA) based on the electrical potential and current density variation within the model by evaluating the smooth and broader distribution within the arm volume conductor. Then, the optimal EA was used to analyze the impedance recording detailed as follows. From the simulation, both the electrical current density and electrical potential variations over the upper arm for different current excitation electrode pairs were investigated.

A. ELECTRICAL CURRENT DISTRIBUTION OVER DIFFERENT EAs

The electrical current density for different EAs is shown in Fig. 5. To compare the EAs based on current density distributions, the minimum range is set 1 mA/m^2. The same settings of the streamline were defined in COMSOL to visualize the current density variation over the arm model-based electrode settings. The results for EA 8 show wider and deeper current density distributions compared to the remaining.

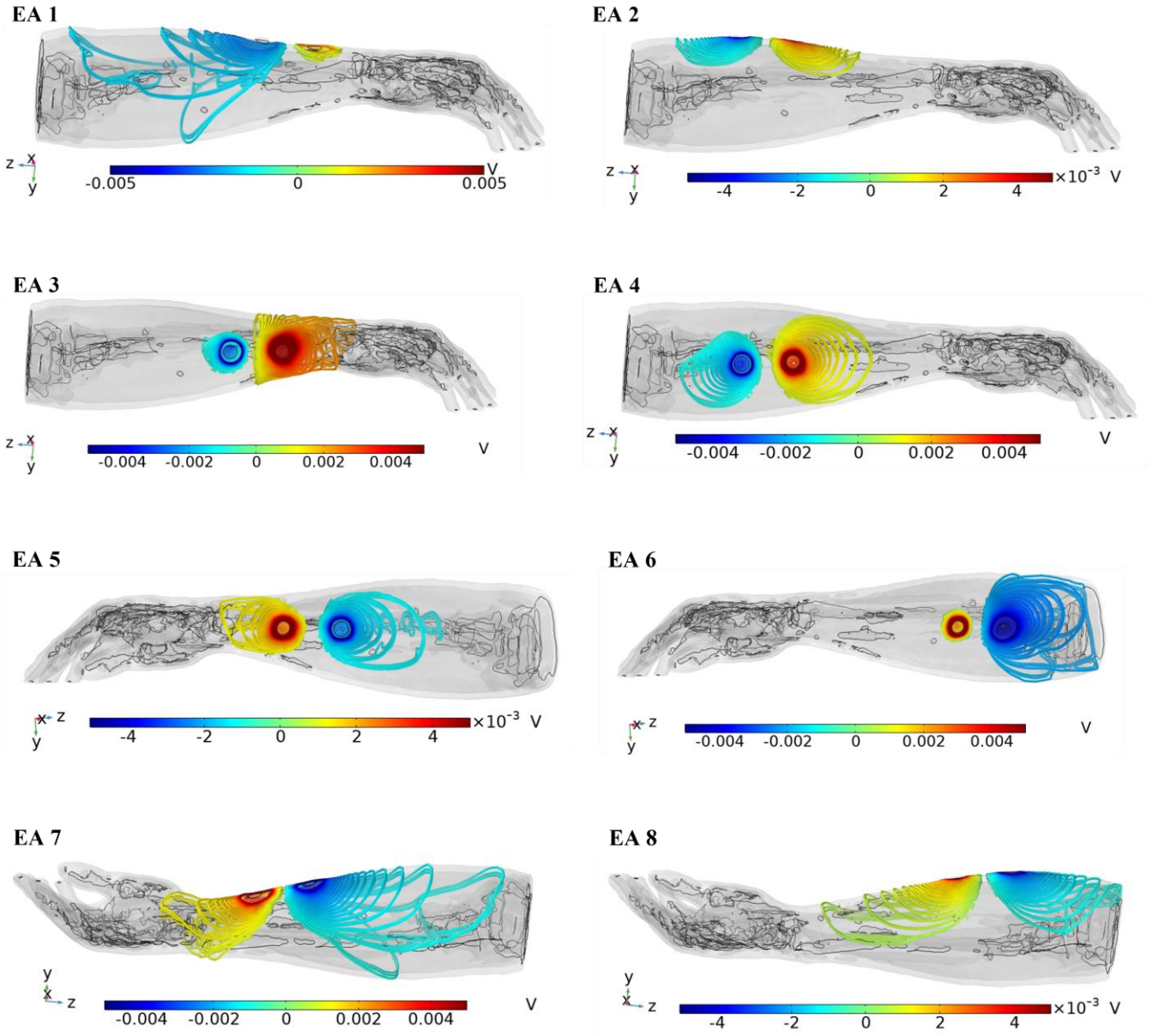

FIGURE 6. **Shows the distributions of the electrical potential variation across the arm model using different electrode arrangements (EAs). The electrical potential distribution contours are highlighted for each EA.**

B. ELECTRICAL POTENTIAL DISTRIBUTION OVER DIFFERENT EAs

For impedance measurements, eventually, the developed voltages are measured. Hence the electrical potential variation over the upper arm for different current excitation electrode pair placements is also looked at. For comparison, electrical potential contours are clamped from ± 0.1 mV to ± 0.5 V. However, the color range is set to ± 0.5 mV to make a clearer difference between polarities as shown in Fig. 6.

The results for EA 2, EA 4, and EA 8 clearly have smooth electrical potential variation compared to the remaining EAs. However, the results for EA 8 have wider electrical potential variation over the arm and it is spread inner layers more than EA 2. Although the negative polarity of EA 1 and EA 7 shows wider electrical potential variation. This is not valid for the positive polarity. Also, this wider variation does not have smooth electrical potential within and over the arm. Although the results for the positive polarity of the EA 3 cover the whole wrist of the arm, this is not valid for the negative polarity. Although the negative polarity of the EA 6 has wider electrical potential variation through the anatomical layers in the vicinity, the same trend is not observed for the positive polarity.

The electrical potential is more penetrated within the arm model and spread over the arm using bottom EAs (EA 7 and EA 8) compared to others. By comparing the bottom EAs, EA 8 is considered an optimal electrode arrangement as it

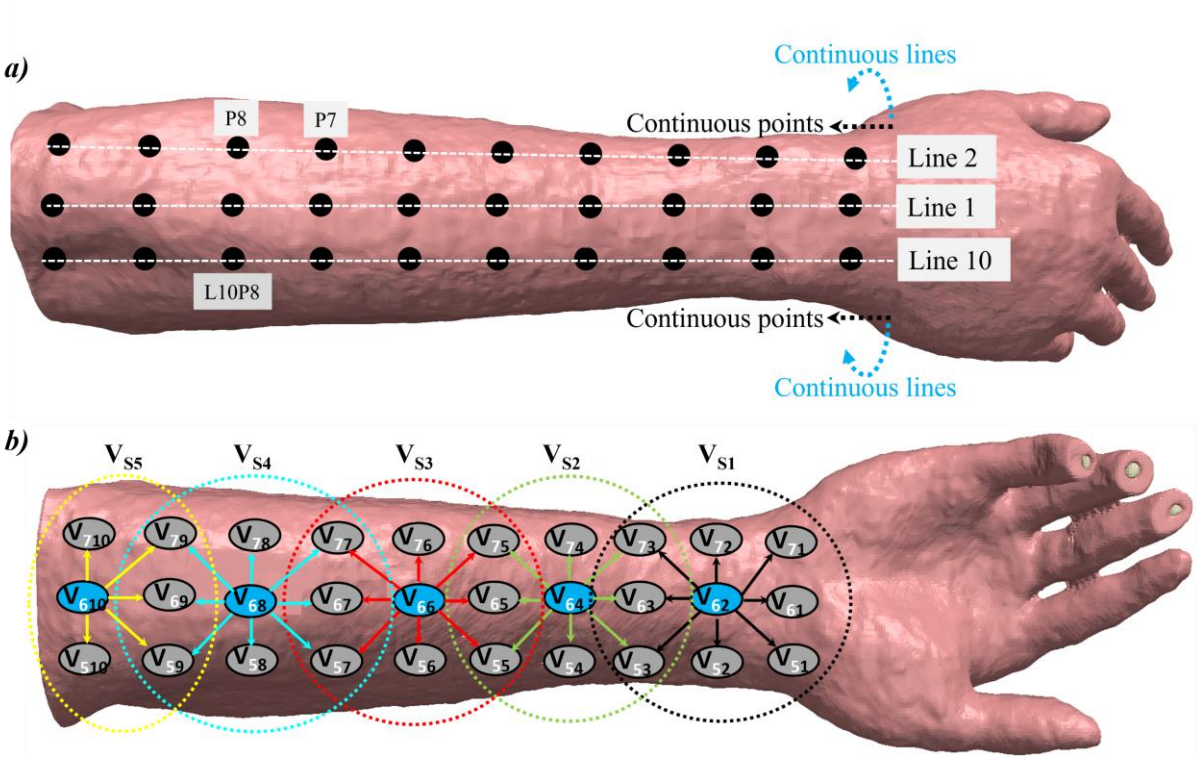

FIGURE 7. (a) The electrical potential recording points and lines are shown. Ten different lines over the arm are generated and each line includes ten different impedance recording points. L10P8: Line 10, point 8. (b) Shows the impedance recording procedures by calculating the electrical potential difference between the neighbors' points. Each recording scenario is highlighted in a different color. The location of the center point is highlighted in blue.

has smooth and wider electrical potential variations.

C. RECORDING PROCEDURE AND BIOIMPEDANCE EXTRACTION

Since it was aimed to derive a map of the impedance variation at various places of the upper arm, the impedance recording position was defined based on systematic procedures using defined optimal EA. Ten different lines (as shown in Fig. 7(a); Line 1, Line 2, …, Line 10) were generated around the upper arm by keeping constant z coordinate; and varying x and y coordinates. Then, ten different points (Point 1, Point 2, …, Point 10) were chosen over each line by following incremental steps from the wrist through the elbow, as highlighted in Fig. 7(a).

The second step of the study was to identify the optimal recording location over the upper arm based on the optimal EA. Thus, a systematic approach was used as follows. The electrical potential difference was calculated between two points using an anticlockwise direction for each voltage recording scenario, as shown in Fig. 7(b). The electrical potential difference was calculated using (4) for the each Vs. The following procedures were applied: i) the center point (highlighted in blue in Fig. 7b) was defined for each Vs. ii) the electrical potential difference was calculated using subtraction between the center point and all neighbor points' electrical potential by following the anti-clock direction. This was repeated for all Vs. All Vs have eight electrical potential variation (as shown in (4)) apart from the last Vs. It is noted that the voltage difference was saved as a sinusoidal waveform for each Z = Vs/I.

$$V_{S1} = \begin{bmatrix} V_{62} - V_{61} & V_{62} - V_{71} & V_{62} - V_{72} & V_{62} - V_{73} \\ V_{62} - V_{63} & V_{62} - V_{53} & V_{62} - V_{52} & V_{62} - V_{51} \end{bmatrix} \quad (4)$$

Where V_{S1} shows the electrical potential difference between the neighbors' points based on the defined recording scenario, V_{xy}, x represents line number and y indicates point number. Rest of the voltages were recorded using the same measurement pattern.

Then, the impedance value for each V_S was recorded by dividing the sinusoidal voltage difference by the sinusoidal current. Eight different impedances were calculated by taking electrical potential difference for each V_S (five variations was recorded for the last V_S for each arm side as highlighted in yellow in Fig. 7(b) using optimal EA). This resulted in 37 impedance recordings for a side of the upper arm (e.g., the bottom side). The recording method was applied to four different sides (top, bottom, right, and left) of the arm using the same procedures as shown in (4). Thus, in total, 20 different Vs (V_{S1} to V_{S20}) and 148 impedance variations were recorded based on the optimal EA using the electrical potential difference between two points along the upper arm. The phase was measured by the delays between the recorded Vs and injection current sine wave forms.

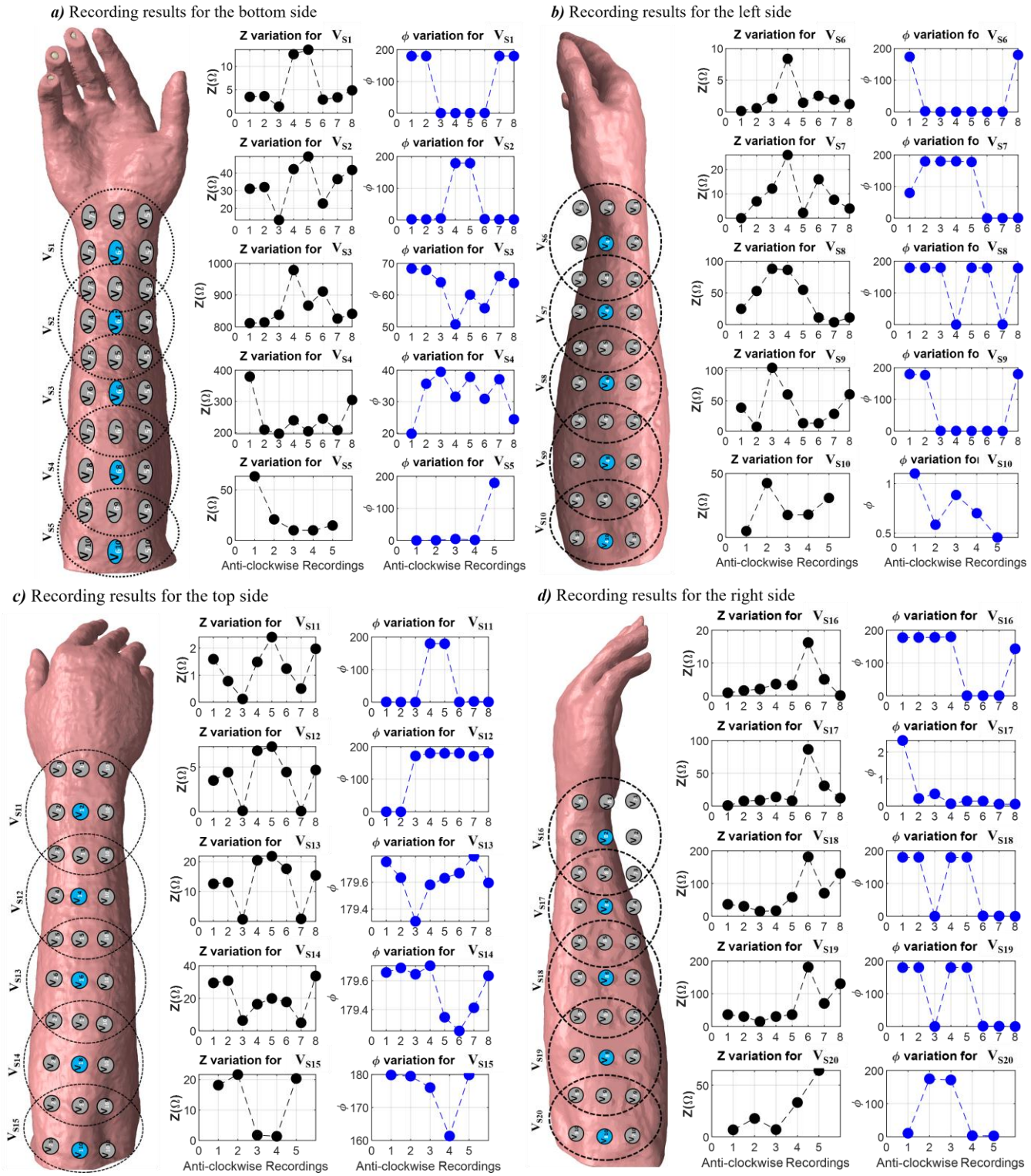

FIGURE 8. Showing impedance and phase variation versus anti-clock recording scenario (Rs) by calculating the electrical potential difference between the recording points over the arm model using the optimal electrode arrangement. The impedance and the phase variations are shown for the bottom (a), left (b), top (c), and right (d) sides of the upper arm. It is noted that the position of the recording points is approximated. Φ shows the phase difference.

The results for the impedance and phase values based on different recording scenarios over the arm using the optimal EA are shown in Fig. 8. The results for the bottom (a), left (b), top (c), and right (d) sides of the arm are highlighted.

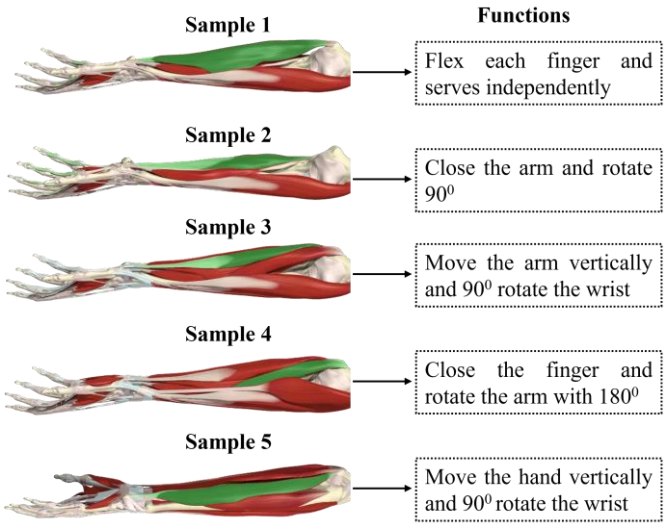

FIGURE 9. **Fig. 9. Shows muscle samples anatomy at the bottom of the arm territory and their functions. Using EA 8 may be possible to control these arm movements.**

The maximum recorded impedance value is about 1 kΩ and the phase difference varies between 0° to 200°.

The impedance and phase variation for the bottom side of the arm based on five different V_S (V_{S1} to V_{S5}) is shown in Fig. 8(a). It is clearly shown that there is a significant fluctuation in both impedance and phase variations. In most cases, when the impedance variation shows an increase, the phase difference variation shows the opposite trend. The impedance variation is relatively higher for the V_{S3}, the value is between 800 Ω to 1 kΩ. The impedance variation for V_{S1} and V_{S5} is comparatively lower. The recording range is about 2 Ω to 50 Ω. The phase difference varies between 0 – 200. The results of V_{S3} and V_{S4} show higher impedance values. This is largely due to the injecting EA positions.

The impedance and phase variation for the left side of the arm based on five different V_S (V_{S6} to V_{S10}) is shown in Fig. 8(b). Although there is no linear increase or decrease in the magnitude of the impedance and phase difference based on anti-clock recordings, in general, the magnitude values of the impedance are higher for the recording points that are close to the bottom side of the arm. The impedance range is 2 Ω to 100 Ω. It is shown that the maximum impedance V_S is that of V_{S8} and V_{S9}.

The impedance and phase variation for the top side of the arm based on five different V_S (V_{S11} to V_{S15}) is shown in Fig. 8(c). There is a significant reduction in the impedance variation compared to the other recording sides of the arm. The impedance range is 2 Ω to 20 Ω. The relative impedance recording position is identical to the other recording sides.

The impedance and phase variation for the right side of the arm based on five different V_S (V_{S15} to V_{S20}) is shown in Fig. 8 (d). Interestingly, the impedance variation and the phase difference are identical for V_{S18} and V_{S19}. Although the phase difference variation is quite different, the impedance variation shows the same trend for V_{S16} and V_{S17}. However, the impedance results are relatively higher for V_{S17} compared to V_{S16}. The higher value of the impedance is recorded for V_{S18} and V_{S19}.

Overall, as can be observed in Fig. 8, for EA 8, relatively higher values of the impedance are obtained at the location that is close to the elbow for all impedance recording sides of the arm.

IV. DISCUSSION

It is not feasible to investigate the impact of the various EAs on the impedance variation of BIA of the upper extremity using the experimental test due to the variation of both geometrical and electrical parameters. It has been shown that dielectric properties of biological tissues, the anatomy of the body part around the muscle of interest, and the anatomy of the muscle itself have a considerable effect on the measured impedance. Thus, bio-computational models can be used in the design and development of BIA strategy in various applications by considering such variations [11], [13], [19]–[21].

The fundamental goal of this study was to perform a quantitative evaluation of a range of EAs on the impedance variation for BIA of HMI using computational modeling procedures as the process summarized in Fig. 1. Thus, the first step of this study was to identify the optimal EA based simulating larger area of the target muscle. As shown in Fig. 2, various EAs were generated and systematically placed over the upper arm to identify the most appropriate one for the BIA of HMI based on electrical potential and current density distributions. The impedance, phase difference, and induced electrical potential variations were calculated using appropriate boundary conditions and dielectric properties of the associated tissue layers based on the transient solution method. The results showed that EAs have a significant impact on the impedance, phase, and distribution of the electrical potential variation across the arm. The electrical current density results in Fig. 5 and the results for the potential results in Fig. 6 showed that EA 8 can be chosen as the optimal electrode based on the defined criteria. It was also shown that the recorded impedance range was in agreement with the existing study [22].

When the results based on the electrical potential and current density were considered for all EAs, the results for EA 8 indicated that the electrical potential was evenly distributed in the vicinity of the electrode and transmitted to the inner layers. This may be associated with the amount of the smooth distribution of muscle layer in this region. Since the conductivity of the muscle layer is relatively higher as shown in Table 1, the induced electrical potential showed smooth variation in this region. Also, Fig. 9 showed that the muscle in this region has a significant role in controlling hand movements (Anatomy.tv., Database, UCL). Thus, EA 8 can be considered as an optimal EA based on these factors.

The impedance values can be analyzed for the control most of hand movements. Therefore, the second step of this study was to analyze the optimal recording location of the human arm using optimal EA. As shown in Fig. 7, a methodology was proposed for the optimization of the

impedance recording location over the arm using BIA. The results for this were shown in Fig. 8 based on different locations of the arm using optimal EA. It is clearly shown that the magnitude of the impedance was higher in the location where it was close to the elbow of the arm for all recording sides of the arm. Apart from the impact of current densities, this may be related to the fact that the origin of the associated muscle is close to the elbow of the arm as samples indicated in Fig. 9. The impedance variation trend was the same for all recording sides as the impedance value was increased from the wrist towards the elbow of the arm then, it started to suddenly decrease at the vicinity of the elbow. This may be related to the amount of soft tissue in this region and the location of the electrode placement over the arm. This is also reflected on recorded impedance values being slightly higher for the right side of the arm compared to the left side. Despite the impedance variation showed a similar trend for most of the V_S as shown in Fig. 8 (b), (d), the anatomical thickness is different for the right side of the arm compared to the left side. The lowest impedance variation was recorded for the top side of the arm (shown in Fig. 8(c)) mainly due to the distance between the current injection and recording locations. Even though injection current decayed when the distance is increased as shown in Fig. 5, yet 2 Ω to 20 Ω were recorded. Hence top-side muscles can be easily monitored using low noise recording circuit.

Thus, this study suggested placing the EA on the bottom side that is towards to elbow, for simulating a wide range of the arm muscle. This may help to control multiple movements of the arm and hand as shown in Fig. 9.

V. CONCLUSION

In this study, the multilayer FEM models of the human arm were developed to investigate the impact of electrode placement on impedance, phase, and electrical potential distributions along the upper arm using appropriate boundary conditions and dielectric properties of anatomical layers. The transient solution method was used to obtain more accurate results based on given measurement settings. The results showed that EAs have a significant impact on impedance variation. It was shown that the EAs can be defined based on electrical potential and current density variations along the upper - arm. Since the main aim of the study was to simulate a wide range of the muscle layer, it was shown that recording the BIA at the bottom side of the arm towards the elbow may give the optimal recording strategy. Thus, the results can be used for guiding electrode position in, e.g., large-scale flexible printed electrode placement in BIA.

CONFLICTS OF INTEREST

The authors declared no potential conflicts of interest concerning the research, authorship, and/or publication of this article.

ACKNOWLEDGEMENT

The authors would like to thank UCL library for the financial support.

REFERENCES

[1] A. Fougner, O. Stavdahl, P. J. Kyberd, Y. G. Losier, and P. A. Parker, "Control of upper limb prostheses: Terminology and proportional myoelectric controla review," IEEE Transactions on Neural Systems and Rehabilitation Engineering, vol. 20, no. 5, pp. 663–677, 2012, doi: 10.1109/TNSRE.2012.2196711.
[2] P. F. Pasquina et al., "First-in-man demonstration of a fully implanted myoelectric sensors system to control an advanced electromechanical prosthetic hand," J Neurosci Methods, vol. 244, pp. 85–93, 2015, doi: 10.1016/j.jneumeth.2014.07.016.
[3] Y. Zhang and C. Harrison, "Tomo: Wearable, Low-Cost, Electrical Impedance Tomography for Hand Gesture Recognition," Proceedings of the 28th Annual ACM Symposium on User Interface Software & Technology - UIST '15, pp. 167–173, 2015, doi: 10.1145/2807442.2807480.
[4] Y. Wu, D. Jiang, X. Liu, R. Bayford, and A. Demosthenous, "A Human-Machine Interface Using Electrical Impedance Tomography for Hand Prosthesis Control," IEEE Trans Biomed Circuits Syst, vol. 12, no. 6, pp. 1322–1333, 2018, doi: 10.1109/TBCAS.2018.2878395.
[5] M. A. Trout, A. T. Harrison, M. R. Brinton, and J. A. George, "A portable, programmable, multichannel stimulator with high compliance voltage for noninvasive neural stimulation of motor and sensory nerves in humans," Sci Rep, vol. 13, no. 1, Dec. 2023, doi: 10.1038/s41598-023-30545-8.
[6] G. Gu et al., "A soft neuroprosthetic hand providing simultaneous myoelectric control and tactile feedback," Nat Biomed Eng, Apr. 2021, doi: 10.1038/s41551-021-00767-0.
[7] A. Pradhan, J. He, and N. Jiang, "Multi-day dataset of forearm and wrist electromyogram for hand gesture recognition and biometrics," Sci Data, vol. 9, no. 1, Dec. 2022, doi: 10.1038/s41597-022-01836-y.
[8] E. Salkim, A. Shiraz, and A. Demosthenous, "Impact of neuroanatomical variations and electrode orientation on stimulus current in a device for migraine: A computational study," J Neural Eng, vol. 17, no. 1, 2020, doi: 10.1088/1741-2552/ab3d94.
[9] V. Viswam, M. E. J. Obien, F. Franke, U. Frey, and A. Hierlemann, "Optimal electrode size for multi-scale extracellular-potential recording from neuronal assemblies," Front Neurosci, vol. 13, no. APR, 2019, doi: 10.3389/fnins.2019.00385.
[10] N. Hyv¨onen, H. Hyv¨onen, A. Sepp¨anen, S. Sepp¨anen, and S. Staboulis, "OPTIMIZING ELECTRODE POSITIONS IN ELECTRICAL IMPEDANCE TOMOGRAPHY," 2014.
[11] E. Salkim and Y. Wu, "Anatomical 3D Modeling of Upper Limb for Bio-impedance based Hand Motion Interpretation," pp. 1–4, 2021, doi: 10.1109/fleps51544.2021.9469842.
[12] V. T. Krasteva and S. P. Papazov, "Estimation of current density distribution under electrodes for external defibrillation," Biomed Eng Online, vol. 1, p. 7, Dec. 2002, doi: 10.1186/1475-925X-1-7.
[13] E. Salkim, "Analysis of tissue electrical properties on bio-impedance variation of upper limps", doi: 10.3906/elk-1300-0632.3908.
[14] E. Salkim, "Optimisation of a Wearable Neuromodulator for Migraine Using Computational Methods," Doctoral thesis, UCL (University College London). Feb. 2019.
[15] R. Plonsey and D. B. Heppner, "Considerations of quasi-stationarity in electrophysiological systems," Bull Math Biophys, vol. 29, no. 4, pp. 657–664, 1967, doi: 10.1007/BF02476917.
[16] C. A. Bossetti, M. J. Birdno, and W. M. Grill, "Analysis of the quasi-static approximation for calculating potentials generated by neural stimulation," J Neural Eng, vol. 5, no. 1, pp. 44–53, Mar. 2008, doi: 10.1088/1741-2560/5/1/005.
[17] C. Gabriel et al., "The dielectric properties of biological tissues: I. Literature survey," Phys Med Biol, vol. 41, no. 11, pp. 2231–2249, Nov. 1996, doi: 10.1088/0031-9155/41/11/001.
[18] A. Kuhn and T. Keller, "A 3d transient model for transcutaneous functional electrical stimulation," International Functional Electrical Stimulation Society Conference, vol. 10, no. July, pp. 385–7, 2005,
[19] N. Ravichandran, M. Y. Teo, K. Aw, and A. McDaid, "Design of Transcutaneous Stimulation Electrodes for Wearable Neuroprostheses," IEEE Transactions on Neural Systems and Rehabilitation Engineering, vol. 28, no. 7, pp. 1651–1660, Jul. 2020, doi: 10.1109/TNSRE.2020.2994900.
[20] A. Briko et al., "Determination of the geometric parameters of electrode systems for electrical impedance myography: A preliminary study," Sensors, vol. 22, no. 1, Jan. 2022, doi: 10.3390/s22010097.

[21] A. F. Schrunder, S. Rodriguez, and A. Rusu, "A Finite Element Analysis and Circuit Modelling Methodology for Studying Electrical Impedance Myography of Human Limbs," IEEE Trans Biomed Eng, vol. 69, no. 1, pp. 244–255, Jan. 2022, doi: 10.1109/TBME.2021.3091884.
[22] H. W. Noh, J. Y. Sim, C. G. Ahn, and Y. Ku, "Electrical impedance of upper limb enables robust wearable identity recognition against variation in finger placement and environmental factors," Biosensors (Basel), vol. 11, no. 10, Oct. 2021, doi: 10.3390/bios11100398.

E. SALKIM received the B.S. degree (Hons.) in electrical and electronic engineering from Karadeniz Technical University, Trabzon, Turkey, in 2012, the M.Sc. degree in advanced electronics engineering from Brunel University London, London, U.K., in 2014, and the Ph.D. degree from University College London (UCL), London, in 2019. He was a Research Assistant with the Analog and Biomedical Electronics Group, UCL, in 2018. From 2019-2020, he was a Research Associate with the Analog and Biomedical Electronics Group. He is currently a visiting research fellow and postgraduate teaching assistant. His research interests include the design and development of medical devices using bio-computational modeling and circuit design for wearable and implantable applications. He was a recipient of the Turkish Government Scholarship to pursue his M.Sc. and Ph.D. degrees. He has over 20 publications. He has given many presentations at flagship international conferences and was the session chair for the conference. He is an awardee of the 9th UCL DRA. He is currently an Assistant Professor of Biomedical Electronics.

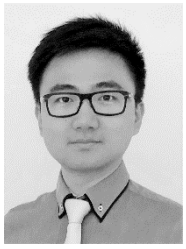

Y. Wu received the B.Eng. degree in electronic and electrical engineering from University College London (UCL), London, U.K., in 2012, the M.Sc. degree in analog and digital integrated circuit design from Imperial College London, London, in 2013, and the Ph.D. degree in electronic and electrical engineering from UCL, in 2019. From 2016 to 2022, he was a Research Associate/Fellow with the Bioelectronics Group, UCL. He is currently a Lecturer with the Department of Electronic and Electrical Engineering, UCL. His current research interests include human-machine interactive systems, CMOS integrated circuit design, and novel mixed-signal microelectronic systems for biomedical applications.